Composites Part B 247 (2022) 110294

Contents lists available at ScienceDirect

Composites Part B

journal homepage: www.elsevier.com/locate/compositesb

A multifunctional nanofiber reinforced photo-crosslinking hydrogel for skin wound healing

Fan Yu [a], Atta ur Rehman Khan [b], Yaqiang Li [c], Binan Zhao [d], Xianrui Xie [a], Mohamed EL-Newehy [e], Hany EL-Hamshary [e], Yosry Morsi [f], Jun Li [d,**], Jianfeng Pan [d,***], Xiumei Mo [a,*]

[a] State Key Laboratory for Modification of Chemical Fibers and Polymer Materials, Shanghai Engineering Research Center of Nano-Biomaterials and Regenerative Medicine, College of Biological Science and Medical Engineering, Donghua University, Songjiang, Shanghai, 201600, PR China
[b] Department of Biotechnology, The University of Azad Jammu and Kashmir, Muzaffarabad, Pakistan
[c] Department of Bone and Joint Surgery, Department of Orthopedics, Renji Hospital, School of Medicine, Shanghai Jiao Tong University, Shanghai, 200001, PR China
[d] Department of Orthopedics, Shanghai Tenth People's Hospital, School of Medicine, Tongji University, Shanghai, 200072, PR China
[e] Department of Chemistry, College of Science, King Saud University, P.O. Box 2455, Riyadh, 11451, Saudi Arabia
[f] Faculty of Engineering and Industrial Sciences, Swinburne University of Technology, Boroondara, VIC, 3122, Australia

ARTICLE INFO

Keywords:
Chitosan
Photo-crosslinking hydrogel
Wound dressing
Antibacterial
Nanofiber

ABSTRACT

Acute skin wounds often lead to tissue defects and bacterial infection, leading to the suffering of patients. In this study, we reported a multifunctional nanofiber reinforced photo-crosslinking hydrogel wound dressing mainly based on natural biomaterials to mimic the structure and components of the native extracellular matrix (ECM). Gelatin-methacryloyl (GelMA), Thioglycolic acid-modified chitosan (TCS) and 3-buten-1-amine (BA) modified polycaprolactone nanofiber (PCLPBA) were prepared and photo-crosslinked into GTP hydrogel. Among all hydrogels, the GTP4 hydrogel possessed rapid liquid-gel transition at ultraviolet (UV) exposure, excellent antibacterial effect, antioxidant property, and printability through 3D printing. Besides, NIH 3T3 cells proliferated well and invaded GTP4 hydrogel. When it was applied to the full-thickness skin defect, GTP4 hydrogel showed the enhanced angiogenesis, re-epithelialization and wound healing effect. Therefore, these findings indicate that the GTP4 hydrogel is a promising wound dressing for acute skin wounds.

1. Introduction

Acute skin wounds are injuries that affected millions of people annually worldwide. They lead to skin functional decline and cosmetic troubles that severely affect the life quality of patients [1]. During the treatment of acute wounds, the first aim is to release the pain of patients, prevent microbial infection, and accelerate wound healing to avoid the occurrence of chronic wounds. Although skin graft has been the golden standard of wound defect, the shortage of autologous skin and immune rejection of allogeneic skin limit its application [2]. The application of skin wound dressing could partly offset the above limitation since the wound dressing can greatly improve patient care after debridement, provide a moist environment for the wound bed, ensure sterility and gas exchange, promote angiogenesis and connective tissue regeneration and be easily removed after healing [3].

Due to its inherent high-water content and fluidity, hydrogel is widely used as wound dressing, which could prevent dehydration of wounds and increase granulation formation. Except for infected wounds and severe drainage wounds, hydrogel is suitable for all four stages of wound healing, since it is non-irritating, permeable metabolites and free from biological tissue reaction [4]. Compared with general hydrogel, the photo-crosslinking hydrogel is a promising wound dressing. Its precursor solution can be injected into the irregular wound, achieve rapid gelation *in situ* and relieve pain simultaneously [5]. Presently, various materials have been developed to fabricate photo-crosslinking hydrogels, such as gelatin, chitosan, carboxymethyl cellulose and their derivatives [6]. Besides, most photo-crosslinking hydrogels can meet the patient's need of constructing personalized wound dressings with

* Corresponding author.
** Corresponding author.
*** Corresponding author.
E-mail addresses: lijunspine@163.com (J. Li), pansmith@163.com (J. Pan), xmm@dhu.edu.cn (X. Mo).

https://doi.org/10.1016/j.compositesb.2022.110294
Received 29 May 2022; Received in revised form 30 August 2022; Accepted 9 September 2022
Available online 14 September 2022

complex structure by 3D printing [7].

Currently, hydrogel wound dressing faces some difficulties. The accumulation of tissue exudate leads to maceration and bacterial infection [8]. The low mechanical property makes it difficult to remove from wounds [9]. While the high mechanical property caused by dense crosslinking density may limit cell immigration and invasion [10]. Besides, the lack of ultrastructure and similar chemical components to the natural extracellular matrix (ECM) is bad for the function of adjacent cells during tissue remodeling [11]. Therefore, there is an urgent need for a form of hydrogel so that the effect of wound dressing can be improved. The natural biomaterials-based hydrogel can fit the criteria of components. Most natural biomaterials have wide sources, relatively low prices and similar chemical components. Besides, they are usually rich in reactive amino, carboxyl and hydroxyl groups, which is convenient for chemical modification [12]. In past decades, nanofiber scaffolds fabricated by electrospinning technologies have been extensively studied and already used in clinical applications. They have advantages over other scaffolds in structure similarity to natural ECM, high porosity, drug loading capacity and controlled release [13]. And the hydrogel with nanofiber is treated as a novel scaffold since it possesses the advantages of nanofiber and hydrogel and can better mimic the structure of natural ECM. Besides, studies also indicate that the composite hydrogel can enhance neovascularization and regulate macrophage polarization, which are beneficial for wound healing [14].

In this study, we demonstrate the efficacy and function of a novel multifunctional photo-crosslinking hydrogel with nanofiber for wound dressing. Gelatin-methacryloyl (GelMA) was selected, which was photo-crosslinkable, and shared the similar amino acid composition of gelatin. Thioglycolic acid-modified chitosan (TCS) was synthesized and used as an antibacterial agent. To deeply mimic the ultrastructure of ECM, 3-buten-1-amine (BA) modified polycaprolactone nanofiber (PCLPBA) was added into the hydrogel system after PCL nanofiber fabrication, homogenization, plasma treatment and reaction with BA. We have systematically investigated the physicochemical properties of hydrogels. Besides, the cytotoxicity and wound healing effect of hydrogels were evaluated by cell experiments and full-thickness skin defect model of SD rat.

2. Experimental section

2.1. Materials

Polycaprolactone (PCL) (M_W = 80 KDa), chitosan (95% deacetylation), thioglycolic acid, gelatin, methacrylic anhydride, 3-buten-1-amine (BA) and toluidine blue O (TBO) were purchased from Sigma-Aldrich. DMEM (Dulbecco's modified eagle medium), Phosphate Buffered Saline (PBS), trypsin, and double antibodies were purchased from Gibco Co. Ltd. Calcein-AM/propidium iodide (PI) Double Stain Kit was purchased from Shanghai Yisheng Biotechnology Co. Ltd. Dichloromethane (DCM), dimethyl sulfoxide (DMSO), N-(3-dimethyl aminopropyl)-N′-ethyl carbodiimide hydrochloride (EDC), 1-Hydroxypyrrolidine (NHS), lithium phenyl-2,4,6-trimethyl-benzoyl phosphonate (LAP) and methacrylic anhydride (MAA) were obtained from Shanghai Macklin Biochemical Co., Ltd. Cell Counting Kit-8 (CCK-8) assay were purchased from Beijing Solarbio Science & Technology Co., Ltd. All other chemicals were purchased from Sinopharm Chemical Reagent Co., Ltd.

2.2. Preparation of PCLPBA

PCL nanofibers were prepared by the reported electrospinning method [15]. In detail, the PCL electrospinning precursor solution (15 wt%) was dissolved in DCM/DMSO solution (v(DCM): v(DMSO) = 9: 1). PCL nanofibers films were carried out by electrospinning equipment under 2 ml/h propulsion rate, 20 kV spinning voltage and 15 cm receiving distance. The nanofiber films were dried in a vacuum oven overnight.

PCLPBA nanofiber dispersion was prepared as Fig. 1a showed. The PCL nanofiber dispersions were fabricated by homogenizer (Joyoung; JYL-C022E) at 12000 rpm for 30 min. Then the PCL nanofiber dispersions were washed with DI water and freeze-drying. Next, plasma-treated PCL nanofibers dispersions (PCLP) were obtained by plasma treatment machine (DT-01, Suzhou Omega Machinery Electronic Technology Co. Ltd.) under 60 w and 60 Pa vacuum degree for 5 min at oxygen atmosphere. Especially, the carboxyl content of PCLP was quantified by the TBO method according to previous literature [16]. Finally, the carboxyl group on PCLP was activated by EDC/NHS for 30 min (n (-COOH): n (EDC): n (NHS) = 1: 4: 4). Subsequently, BA was dropwise added into the above solution (n (-COOH): n ($-NH_2$) = 1: 2). After stirring at room temperature for 24 h, the nanofiber dispersions were subsequently washed by water and ethanol. Finally, PCLPBA nanofiber dispersion was freeze-drying for 24 h and stored at - 20 °C.

2.3. Preparation of TCS

TCS was prepared by the reported method [17]. Briefly, chitosan was dissolved in 0.01 M HCl containing EDC and NHS. Thioglycolic acid was dropwise added into the solution and adjusted pH to 5.0. The amide reaction was carried out at room temperature for 6 h. Finally, the as-prepared solution was dialyzed by the gradient of HCl solution (5 mM, 1 mM) for four days, respectively. The TCS was freeze-dried for 24 h and stored at −20 °C.

2.4. Preparation of GelMA

GelMA was prepared by the reported method [18]. Briefly, gelatin was dissolved in 50 °C PBS to prepare 15 wt% gelatin solution. Subsequently, dropwise addition of MAA into gelatin solution. The reaction was carried out at 50 °C for 6 h the as-prepared solution was dialyzed by DI water for three days. Finally, GelMA was freeze-dried for three days and stored at −20 °C.

2.5. Fabrication of hydrogels

The fabrication of hydrogels was shown in Fig. 1b. GelMA was dissolved in PBS to prepare a 15 wt% precursor solution. Then TCS and photo-initiator LAP were added. After agitation overnight, PCLPBA nanofiber and photo-initiator LAP were added to the above solution and stirred for 2 h in dark. The suspension solution was transferred into a mould with 365 nm UV irradiation (100 mW/cm^2) for 100 s. Especially, the ingredients of hydrogels were presented in Table S1. GelMA group represented hydrogel which only consisted of GelMA. GTP0 group represented hydrogel which consisted of GelMA and PCLPBA nanofiber. GTP1, GTP2, GTP4 and GTP8 groups represented hydrogels that consisted of GelMA, PCLPBA and varied concentration of TCS (5 mg/ml, 10 mg/ml, 20 mg/ml and 40 mg/ml, respectively).

3D printing was performed using a desktop rapid printer (PAM-II) from Shanghai Fuchifan Electromechanical Technology Co., Ltd. The precursor solution (GelMA 0.3 g/ml, TCS 40 mg/ml, PCLPBA 10 mg/ml, LAP 10 mg/ml) was placed in a printing syringe with a 20 G printing needle, extrusion rate of 2 mm/s and layer spacing of 0.15 mm. The extrusion of hydrogel precursor solution was carried out with UV light irradiation simultaneously.

2.6. Characterizations

2.6.1. Nuclear magnetic resonance spectroscopy (^1H NMR) analysis

^1H NMR analysis was carried out on Advance 400 Bruker NMR (400 MHz). The solvents for GelMA, TCS and PCLPBA were deuterium oxide (D_2O), D_2O and $CDCl_3$, respectively. All integral peak areas were analyzed by Mestrenova v12.0.2.

2.6.2. Rheological experiment

The rheological tests were performed using a Thermo Fisher rotational rheometer (HAAKE MARS 60 Rheometer) with UV light components. 20 mm parallel plates were used with a 0.2 cm distance between plates. Angular velocity ω was 10 rad/s, and dynamic time scan γ_0 was 1% during light irradiation. The samples were loaded at 37 °C for 600 s for the dynamic modulus test, followed by UV light irradiation for 100 s. Then the light irradiation stopped with dynamic modulus continuing to measure change for another 200 s.

2.6.3. Morphology of hydrogels and cells cultured on the hydrogels

Freshly prepared hydrogels were frozen at −80 °C for 12 h. Then hydrogels were dried in a freeze dryer for three days. The lyophilized hydrogel samples were sprayed with 10 nm thick platinum (6 mA, 45 s) using a gold spraying instrument. SEM images were taken by using a scanning electron microscope (Phenom XL).

2.6.4. Swelling ratio measurement

The swelling ratio of hydrogels was carried out by the gravimetric method. Briefly, cylindrical hydrogels were soaked in PBS overnight to reach the swelling equilibrium at 37 °C and weighted as w_s. Moreover, hydrogels were freeze-drying for 24 h and weighed as w_d. The following equation calculated the swelling ratio of hydrogel:

$$Swelling\ ratio = \frac{w_s - w_d}{w_d} \times 100\ \%$$

2.6.5. Degradation test

PBS and collagenase in PBS solution were used to measure the degradation of GTP hydrogels. The hydrogel discs were weighed after polymerization and recorded as w_0. Subsequently, they were transferred to a container, and 5 ml of PBS or PBS containing collagenase (2 U/mL) was added, and the PBS was mixed with proclin 300 at a concentration of 0.02% to inhibit bacterial growth, and the PBS containing collagenase was changed once a day to maintain the activity of collagenase. The hydrogels were placed in an incubator at 37 °C. The hydrogel was removed from the solution at a given time point, weighed and recorded as w_1, using four independent samples for each time point. The percentage of residual hydrogel mass was calculated as follows:

$$Weight\ remaining\ ratio = \frac{w_1}{w_0} \times 100\ \%$$

2.6.6. Mechanical property test

Newly prepared hydrogels were immersed in PBS for 4 h before the mechanical property test. The hydrogels were prepared into Ø10 mm × 6 mm size cylinders. Then hydrogels were tested under uniaxial compression by a mechanical testing machine (HY–940FS; Shanghai Hengyu Instrument Co., Ltd). The compression rate was 0.5 mm/min. Each group tested three independent samples to obtain stress-strain curves. The Young's modulus of hydrogels was calculated by the curve corresponding to 0–20% strain.

2.6.7. Antibacterial and antioxidant test

Escherichia coli (*E. coli*, ATCC 25922, CAS) and *Staphylococcus aureus* (*S. aureus*, ATCC 25922, CAS) were used as representative Gram-negative and positive bacteria for antibacterial activity test, respectively [19]. Sterilized MHB broth was prepared and cooling to room temperature. Subsequently, the recovered bacteria were added to the broth on a sterile bench and incubated overnight at 37 °C in an incubator at 200 rpm. The sterile hydrogel precursor solution was added to 24-well plates with 0.4 ml per well and UV irradiated into hydrogels. After photo-crosslinking, 10 μL of bacterial suspension (bacteria concentration = 1.0×10^6 CFU/ml) was added to the surface of each hydrogel, 1 ml of the liquid medium was added to hydrogel groups and the tissue culture plate (TCP) group. After incubation at 37 °C for 18–24 h, the colony-forming units on the agar plates and Petri dishes were counted. Each group tested three independent samples.

$$The\ bacterial\ inhibition\ rate = \frac{n_{TCP} - n_{Hydrogel}}{n_{TCP}} \times 100\ \%$$

Whereas n_{TCP} and $n_{Hydrogel}$ represent the number of colonies in TCP group and the hydrogel group, respectively.

0.2 ml of the above bacterial solution was aspirated and placed on LB medium agar plates for plate coating. The above hydrogels were fixed with paraformaldehyde for 2 h, followed by ethanol gradient dehydration and freeze-dried. SEM images were taken after gold spraying.

The 1,1-Diphenyl-2-picrylhydrazine (DPPH) assay measured the antioxidant test according to the previous report [20]. The concentration of DPPH solution was 0.3 mM. Hydrogels of uniformed size (Φ 10 mm × 4 mm) were mixed with 5 ml DPPH solution and kept in dark at room temperature for 30 min. Ascorbic acid (AA) was mixed with 5 ml DPPH solution and chosen for the standard antioxidant group. DPPH solution was chosen as the blank group. The following equation calculated the antioxidant activity:

$$Antioxidant\ activity = \frac{OD_B - OD_H}{OD_B} \times 100\%$$

OD_B is the absorption of the blank group at 517 nm, and OD_H is the absorption of hydrogel groups at 517 nm. Images were taken after 30 min for color change of solution. Each group tested three independent samples.

2.6.8. Cytotoxicity tests

NIH 3T3 cell line was cultured in DMEM medium containing 10% fetal bovine serum and 1% penicillin/streptomycin. Cells were cultivated in an incubator containing 5% CO_2 at 37 °C to reach logarithmic phase proliferation, which were then collected for further use.

The material for preparing hydrogel prepolymer was sterilized by ethylene oxide. The hydrogel precursor solutions were prepared according to the ratio in Table S1. Hydrogel precursor solutions were placed in a 48-well plate for 60 s exposure of UV light to crosslink into a gel. NIH 3T3 cell suspensions at a density of 40k cell/ml was prepared. Then cells were planted on hydrogels with 20 k cell/well, followed by 0.5 ml complete medium added to each well. Besides, cells planted on a culture plate as a normal control group to calculate the cell viabilities [21]. Culture plates were placed in an incubator (37 °C, 5% CO_2). Each group used four independent hydrogels. On days 1, 3 and 5, the hydrogels were processed for cytotoxicity testing and cell fluorescence photographs using the CCK-8 assay and Live & Dead staining (Calcein-AM and propidium iodide (PI)), respectively.

2.7. Application as wound dressing

2.7.1. In vivo wound healing

All relevant animal experiments in this experiment were approved by the Animal Ethics Committee of Tongji University (ID number: SHDSYY-2021-4427). Mature SD rats (200–300 g) were anaesthetized with inhaled isoflurane, followed by the hair on the back shaved. Then full skin defect was established with a diameter of 15 mm. Hydrogel precursor solutions (GelMA, GTP0 & GTP4) were injected into the wound area, irradiating with UV light (365 nm, 9 W) for 60 s. For the control group, the skin defect was not treated by any wound dressing. Experimental animals (3 SD rats per group) were executed at 1, 2 and 3 weeks postoperatively to observe the wound healing. The wound area was calculated using ImageJ (NIH) software with using the following formula.

$$Wound\ area = \frac{S_1}{S_0} \times 100\ \%$$

Whereas S_0 was the initial wound area, and S_1 is the wound area at different time points.

2.7.2. Histopathological study

Histological staining was performed on the 7th, 14th and 21st day following the creation of the wound. The wound and surrounding tissue were resected, rinsed with PBS, fixed in 4% paraformaldehyde, and then

immersed in paraffin. 5 μm sections of skin tissue were cut, dehydrated and stained with hematoxylin-eosin (H&E) to observe various histological changes such as re-epithelialization and granulation tissue formation. Also, tissues were stained with Masson's trichrome to observe collagen deposition and neointima formation during the healing process. Images were taken by light microscopy. The site with the largest diameter of the wound bed section was selected and images with normal skin on the left and right sides were taken for comparison.

2.7.3. Immunohistochemical study

Immunohistochemical staining of CD31 was performed on 21st day following the creation of the wound. For antigen recovery, the deparaffinized and rehydrated tissue areas were incubated with citric acid (PH = 6.0) solution in a microwave oven for 5 min followed by cooling at room temperature for 30 min and rinsing in 0.01 M PBS for 5 min 3 times. To block endogenous peroxidase and serum, slides were sequentially treated with 3% H_2O_2 for 25 min in the dark and 3% BSA for 30 min at room temperature. The primary antibody, CD31 primary antibody, was put and incubated at 4 °C overnight. The biotinylated goat antirabbit (1:200) was then added and incubated for 30 min at room temperature. The slides were incubated with DAB and H_2O_2 solution for visualization. Slides were counterstained with hematoxylin for 1min, followed by dehydration in sequential ethanol before sealing. All slides were viewed with a CIC XSP-C204 fluorescence microscope.

2.8. Statistical analysis

Comparative analysis of data was performed using origin 2018, and results were expressed as mean ± standard deviation. Significant differences were obtained using one-way ANOVA, Turkey test, which considered *P < 0.05 as statistically significant differences between samples. At **P < 0.01, there is a statistically moderate significant difference between samples. ***P < 0.001, there is a statistically highly significant difference between samples. Error bars represent the standard deviation values for 3–5 samples.

3. Results and discussion

3.1. Preparation of PCLP nanofiber dispersions

PCL nanofiber membranes were first prepared by electrospinning technique. Results showed that PCL nanofiber randomly arrayed with average diameter of 805 nm (Figs. S1e and f). Then the nanofiber was treated by homogeneous breaking and plasma treatment of O_2 (Fig. 1a). Result showed that the water contact angle of membranes changed from 116.8° to 0° (Figs. S1a and b), indicating that the PCL nanofiber changed from hydrophobic to hydrophilic after plasma treatment. This was in consistence with previous study and beneficial for cell attachment [14]. The color of the nanofiber membrane also changed from white to pale yellow (Figs. S1c and d). When placed in PBS, PCLP nanofiber dispersions segregated evenly showing irregular extension with no nanofiber entanglement observed (Fig. 2a), which made it possible for nanofiber composite hydrogel. They were loosely packed and appeared curled (Fig. 2b), which were apparently different from the dense alignment and extension state of nanofiber membrane (Fig. 1a). Statistical analysis of nanofiber length showed that the PCLP nanofibers were in the range of 13–160 μm. The average length of nanofibers was 44 μm (Fig. 2c), close to cell size. Carboxyl groups were introduced on the surface of PCL nanofibers through oxygen plasma treatment (Fig. 2d), and the carboxyl group content on the PCLP surface was quantified by toluidine blue O (TBO) assay [16]. The optical density value (OD value) of known concentrations of TBO in the acetate solution was used for the standard curve (Fig. 2e). By adjusting the plasma treatment time, the content of the carboxyl group on the PCLP surface increased from 45 to 350 nmol/mg, where the 5 mins' treatment had the highest carboxyl group concentration (Fig. 2f). Therefore, 5 mins' plasma treatment was chosen as the standard in subsequent experiment to ensure the hydrophilicity of nanofiber. The length and hydrophilicity of PCLP nanofiber made it suitable for follow-up chemical modification.

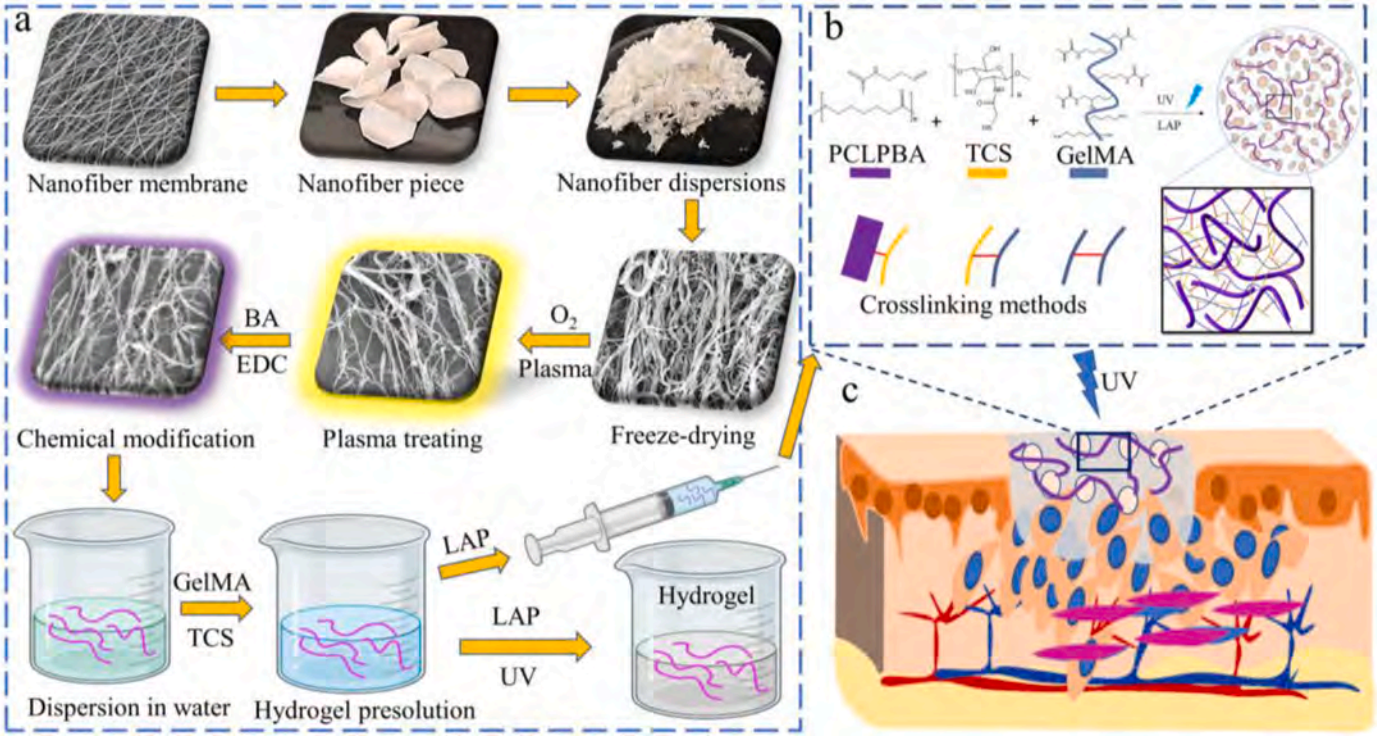

Fig. 1. Schematic illustration of the hydrogel preparation. **a.** Preparation of hydrogel and hydrogel precursor solution. **b.** Chemical composition of the hydrogel precursor solution. The purple, yellow and blue lines indicate PCLPBA, TCS and GelMA, respectively. The red bar indicates interfacial bonds. **c.** Hydrogel formation in wound area.(For interpretation of the references to color in this figure legend, the reader is referred to the Web version of this article.)

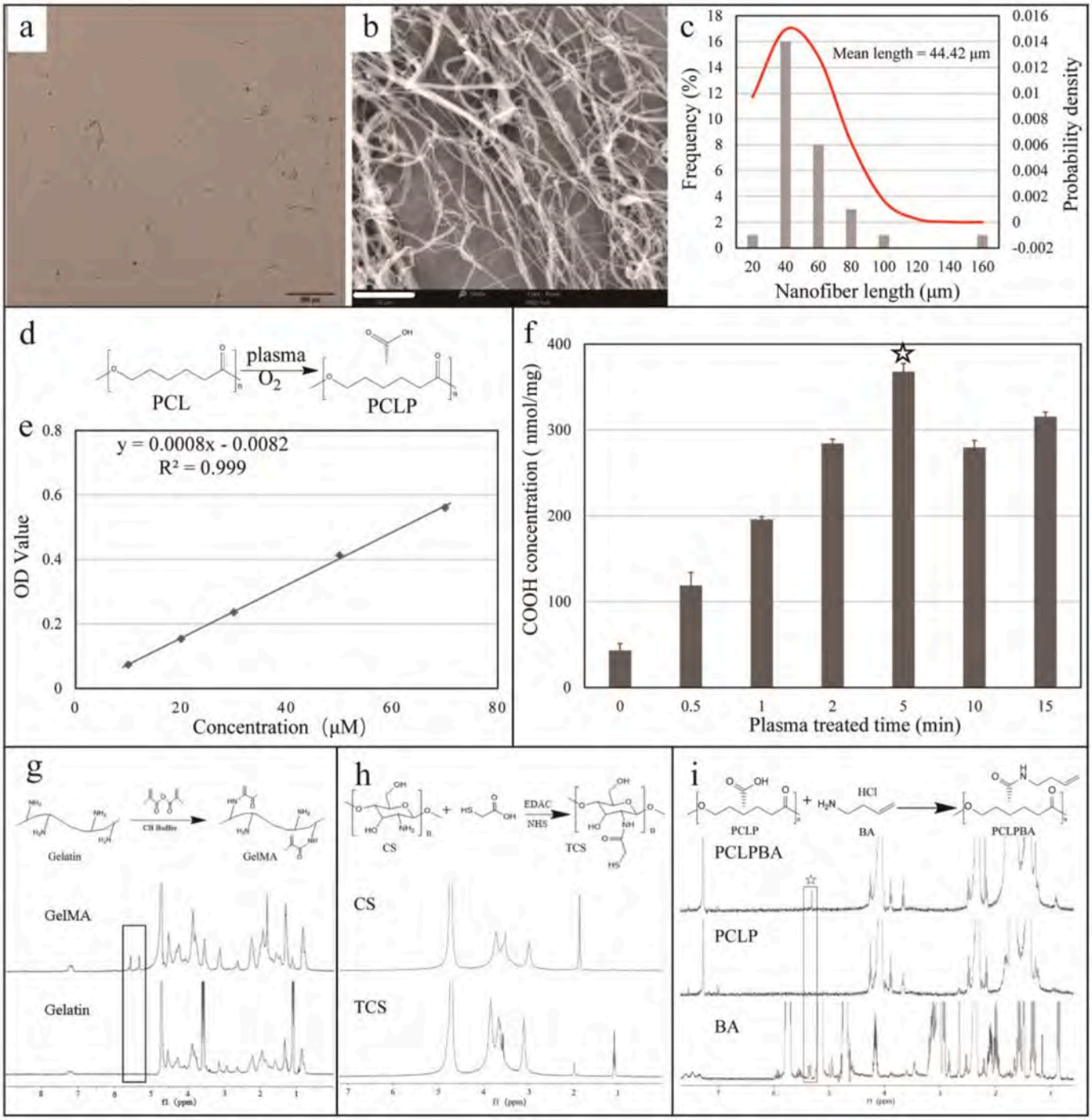

Fig. 2. Fabrication of PCLP nanofiber, GelMA, TCS and PCLPBA. **a**. Optical image of PCLP nanofiber dispersion in deionized water. Scale bar is 200 μm. **b**. SEM image of PCLP nanofiber. Scale bar is 10 μm. **c**. Length distribution of nanofiber. **d**. Chemical schematic of plasma treatment. **e**. Standard curve of O-toluidine blue (TBO) staining method. **f**. Controlling carboxyl group content by changing the plasma treated time. **g.** Preparation of GelMA and its ^{1}H NMR spectra. **h**. Preparation of TCS and its ^{1}H NMR spectra. **i**. Preparation of PCLPBA and its ^{1}H NMR spectra. PCLPBA, PCLP and BA dissolved in $CDCl_3$, $CDCl_3$ and D_2O, respectively.

3.2. Preparation of GelMA, TCS and PCLPBA

GelMA was synthesized as previously reported [21]. Briefly, gelatin was dissolved in PBS, then reacted with methacrylic anhydride. Fig. 2g showed that the peak at 5.3 ppm corresponded to acrylic acid proton grafted on lysine of gelatin. The peak at 5.2 ppm corresponded to the acrylic acid proton, which grafted on hydroxylysine in gelatin with a grafting rate of 64.4%. This result was consistent with the previous report [21]. GelMA shared same components as gelatin. Besides, its solution could be photo-crosslinked in less than 60 s under UV exposure, which has been widely used in wound healing application [22].

TCS was prepared as previously reported [17]. Briefly, chitosan was dissolved in acetic acid solution (2 *wt*%). Then thioglycolic acid and EDAC were added for reaction in dark. As shown in Fig. 2h, new peaks appeared at 1.1 ppm of TCS spectra, corresponding to the absorption peak of the thiol group. Peak intensity decreased at 2.0 ppm corresponding to the amino group on the chitosan backbone. The change of peak intensity at 2.0 ppm indicated that thioglycolic acid reacted with

the amino group. TCS had good electrostatic interaction, negligible cytotoxicity and outstanding antibacterial ability at a concentration of 4 mg/ml. Besides, TCS could function as an antioxidant agent due to its thiol group, which might reduce free radicals and promote wound healing [23].

The PCLP nanofiber was dispersed in distilled water with being activated by EDC and NHS for 30 min. BA was then added to prepare PCLPBA. ^{1}H NMR spectra were acquired from PCLPBA, PCLP and BA dissolved in $CDCl_3$, $CDCl_3$ and D_2O, respectively. Fig. 2i showed that the specific peak of BA was 5.1 ppm, which belonged to methylene protons. A new peak appeared at 5.3 ppm of PCLPBA, which corresponded to the protons of the double bond on BA (☆). It indicated that BA grafted on PCLP nanofiber successfully. Hydrogels with PCLPBA can better mimic the ultrastructure of natural ECM. During the gelation process, PCLPBA might conjugate with GelMA and TCS network, forming an integrated composite structure through interfacial covalent bonds. Plus, it is reported that hydrogels with nanofiber promote cell immigration, significantly reduce fibrosis and scar tissue formation during wound healing, while allowing cell penetration and facilitating angiogenesis [24].

3.3. Morphology of hydrogel and 3D printing structure

Hydrogel precursor solution were photo-crosslinked with UV light and lyophilized for SEM characterization. Result showed that GelMA hydrogel was transparent with smooth surface (Fig. 3a). GTP0 hydrogel was white with visible fibers dispersing evenly inside (Fig. 3b). As for hydrogels with TCS (Fig. 3c–f), hydrogels were opaque. Besides, hydrogel changed from white to yellow with TCS concentration increasing (Fig. 3c, 3d, 3e & 3f). SEM images showed that a dense and porous structure appeared on all hydrogels. PCLPBA was uniformly distributed in both GTP0 and GTP1 hydrogel with no nanofiber entanglement observed, forming an integrated structure. Penetrating pores appeared in GTP2, GTP4 and GTP8 hydrogel. The pore size decreased with TCS, while the wall thickness increased with TCS because of dense network within hydrogels. Suitable pore size and porous structure of hydrogel could facilitate diffusion of air, nutrients, metabolite and cells migration, which is beneficial to wound healing [25]. Hydrogels, except GTP8, represented porous structure with moderate size (Fig. 3a–f), which could satisfy the needs.

Generally, solid components, like nanofiber and nanoparticle, will decrease the flowability of solution and may cause aggregation or entanglement [26]. To test the injectability, hydrogel precursor solution was placed in a syringe with a 20 G needle. Video S1 showed that it had uniform color and could be extruded continuously from needle. Fabrication of hydrogel structure by 3D printing was a best option for personalized healthcare, where the conjugation of bioactive molecules and encapsulation of stem cells were required [27,28]. Therefore, the solution was applied in a 3D printer with UV exposure for gelation

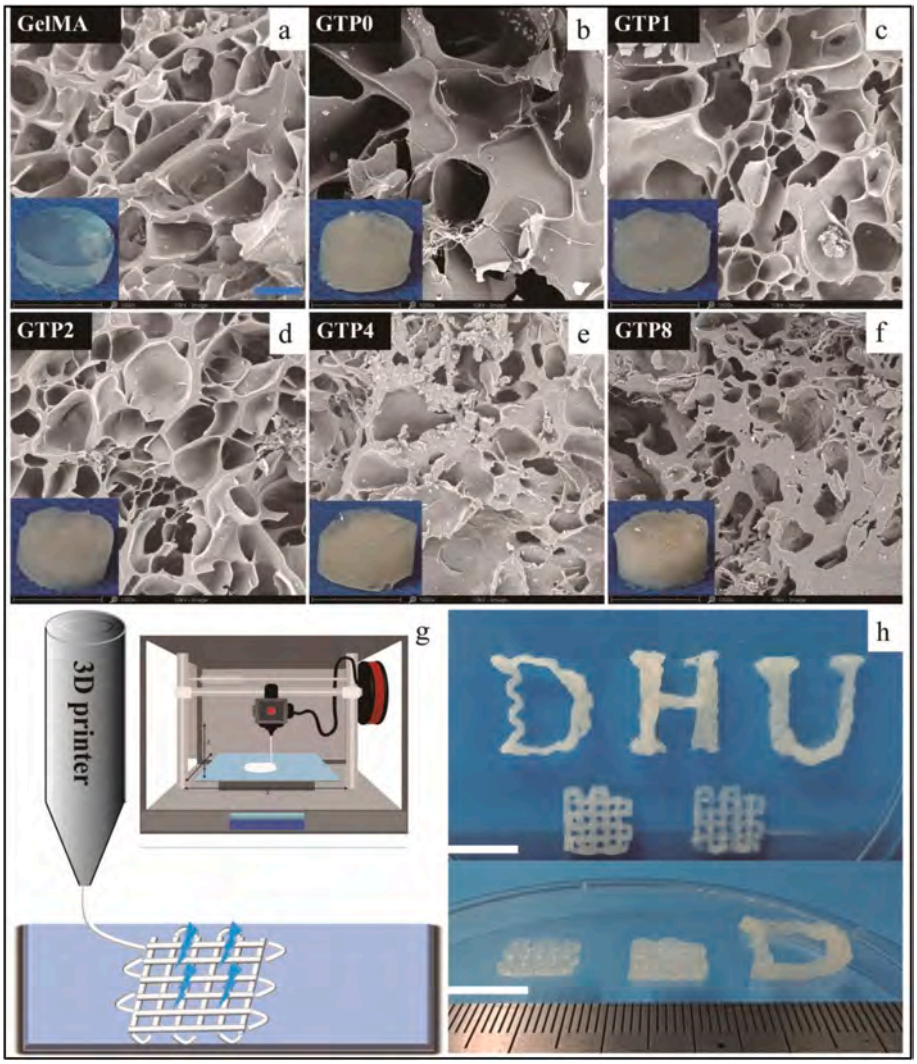

Fig. 3. Morphology of lyophilized hydrogels and optical images of hydrogels. Scale bar is 40 μm. **a**. GelMA hydrogel. **b**. GTP0 hydrogel. **c**. GTP1 hydrogel. **d**. GTP2 hydrogel. **e**. GTP4 hydrogel. **f**. GTP8 hydrogel. **g**. Schematic illustration of hydrogel 3D printing with UV irradiation. **h**. 3D Printed structure. Scale bar is 10 mm.

simultaneously. Result showed that it could be 3D printed into predetermined shape from single layer to multilayer (Video S2, Fig. 3g & h), This may be the consequence of good properties of PCLPBA, such as moderate length (44 μm) and good hydrophilicity. SEM results showed that porous structure was observed on the hydrogel. All components conjugated well without phase separation between TCS and GelMA (Figs. S2a and b). PCLPBA was dispersed evenly inside (Fig. S2c). The results indicate that the composite hydrogel can be used in bio-fabrication and have potential in personalized medicine.

Supplementary video related to this article can be found at https://doi.org/10.1016/j.compositesb.2022.110294

3.4. Mechanical and in vitro degradation properties of hydrogel

The fabricated hydrogels were immersed in PBS for 2 h and then characterized through mechanical tests. Fig. 4a showed that all hydrogels could be compressed up to 45% strain. Young's modulus of hydrogels gradually increased with TCS addition (Fig. 4b). The Young's modulus of GelMA, GTP0 and GTP1 group were 20.6, 29.9 and 36.8 kPa, respectively. The Young's modulus of GTP2, GTP4 and GTP8 were 49.2, 53.9 and 95.5 kPa, respectively. The compression strength of GTP0 was higher than GelMA, which were 27.3 kPa and 19.5 kPa (Fig. 4c), respectively. The compression strength of GTP1, GTP2, GTP4 and GTP8 were 61.5, 78.3, 106.4 and 132.5 kPa, respectively. Hydrogel with moderate network density could provide appropriate mechanical strength, which is vital to match the strength of native tissue, provide wound protection and keep bacterial from invading [29,30]. Young's modulus of hydrogel is below 100 kPa (Fig. 4b), which is close to native adipose tissue [31]. The results indicated that the addition of PCLPBA and TCS could enhance the mechanical strength of hydrogel.

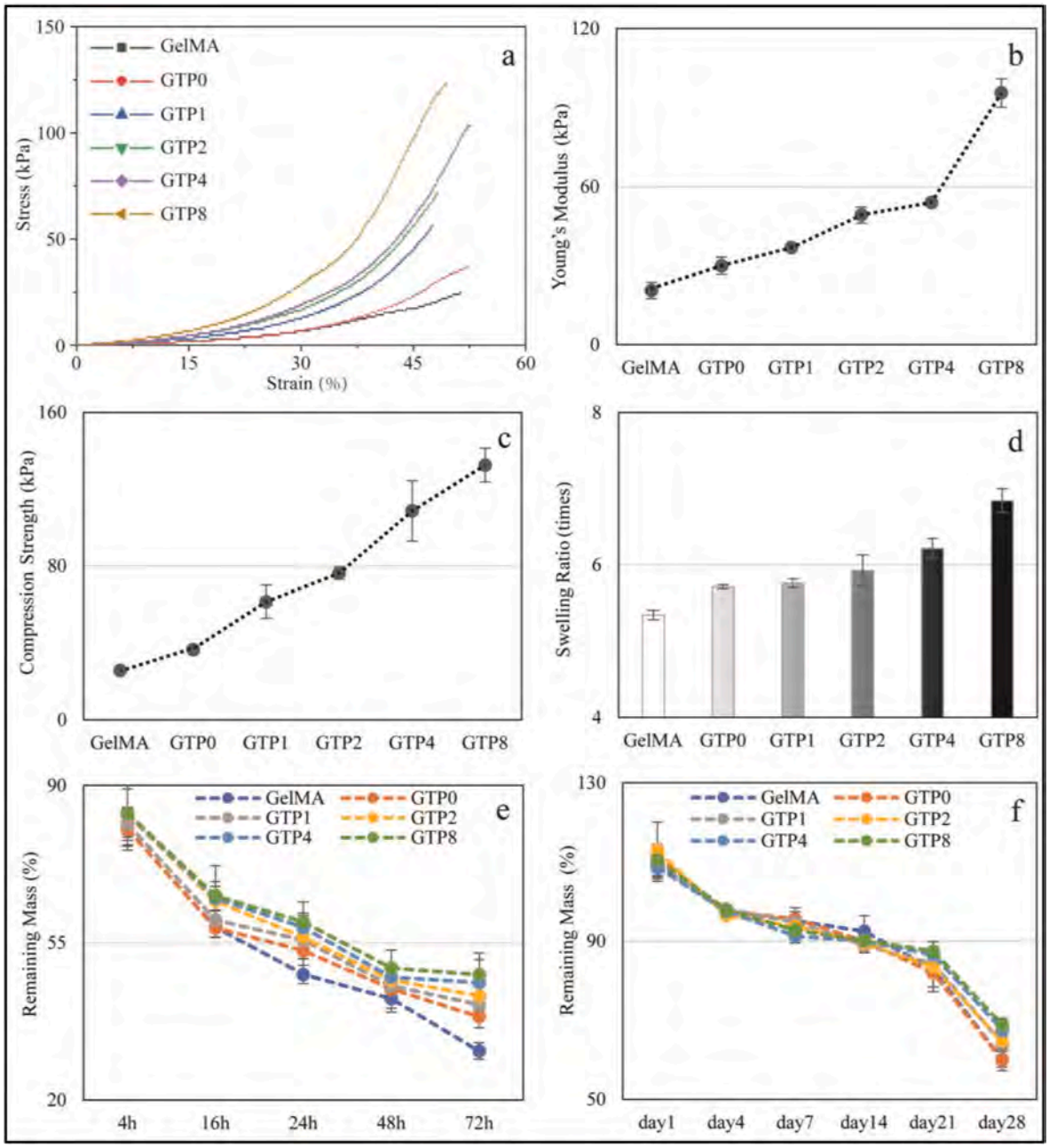

Fig. 4. Mechanical properties of hydrogels. **a**. Stress-strain curves of hydrogels. **b**. Young's modulus of hydrogels. **c**. The compression strength of hydrogels. **d**. The swelling ratio of hydrogels. **e.** Hydrogel degradation in collagenase solution. **f.** Hydrogel degradation in PBS.

Additionally, the swelling ratio of hydrogels was tested. Fig. 4d showed that the ratio of GelMA and GTP0 hydrogel were 5.3 and 5.7, respectively. And the ratio of GTP1, GTP2, GTP4 and GTP8 hydrogels were 5.75, 5.92, 6.2 and 6.8, respectively. The results indicated that PCLPBA and TCS improved the swelling ratio of GelMA hydrogel, which was in consistence with previous study [32].

The degradation properties of the scaffold were closely related to tissue regeneration. The *in vitro* degradation property of hydrogels was characterized by using collagenase PBS solution and PBS, respectively. As demonstrated, the mass remaining ratio of hydrogels decreased gradually (Fig. 4e and f). At 72 h, the remaining mass of hydrogels in collagenase PBS solution were below 50%. The remaining mass of GelMA was lowest among all groups. The remaining mass of GelMA and GTP0 were 26.4% and 39.5%, respectively. While the remaining mass of GTP1, GTP2, GTP4 and GTP8 were 41.2%, 43.1%, 46.1% and 47.9%, respectively. The remaining mass of hydrogels in PBS also decreased with time (Fig. 4f). On day 1, hydrogel mass increased slightly due to the swelling of hydrogels. The remaining mass of GelMA, GTP0 and GTP1 were 109.4%, 111.2% and 110.2%, respectively. The remaining mass of GTP2, GTP4 and GTP8 were 112.8%, 108.6% and 110.5% respectively. On day 28, the remaining mass of GelMA, GTP0 and GTP1 hydrogel were 60.0% 59.9% and 64.3%, respectively. The remaining mass of GTP2, GTP4 and GTP8 hydrogel were 64.6%, 67.5% and 68.8%, respectively. The results indicated that all hydrogels were degradable. Besides, hydrogels with more TCS (GTP4 and GTP8) showed higher mass remaining ratio, which was attributed to the denser network inside.

3.5. Rheological properties

The rheological properties of hydrogels were investigated by dynamic rheological test upon 365 nm light irradiation. Fig. 5a and b showed that the storage modulus (G′) and loss modulus (G″) of all hydrogel precursor solution remained low in the initial phase (0–600 s). In the photo-crosslinking phase (600–700 s), G′ and G″ rose sharply, indicating precursor solutions turned into hydrogels. In the final phase (700–900 s), G′ and G″ of hydrogels continued to increase, which was more evident in hydrogels containing TCS. Statistical analysis of G′ and G″ showed that PCLPBA and TCS led to the increase of G′ and G" (Fig. 5a and b). G′ of GelMA, GTP0 and GTP1 hydrogels were 342.4 Pa, 679.2 Pa and 913.1 Pa, respectively. While the G′ of GTP2, GTP4 and GTP8 hydrogels were 1165.7 Pa, 1582.6 Pa and 2906 Pa, respectively. G″ of GelMA, GTP0 and GTP1 hydrogels were 6.4 Pa, 13.9 Pa and 37.0 Pa, respectively. While the G″ of GTP2, GTP4 and GTP8 hydrogels were 68.5 Pa, 87.9 Pa and 125.8 Pa, respectively. The results indicated that precursor solutions could form hydrogel after UV irradiation for 100 s, which might satisfy the requirement of clinical operation [33].

3.6. Antibacterial test

After being cultured overnight, 200 μL of bacterial was taken from

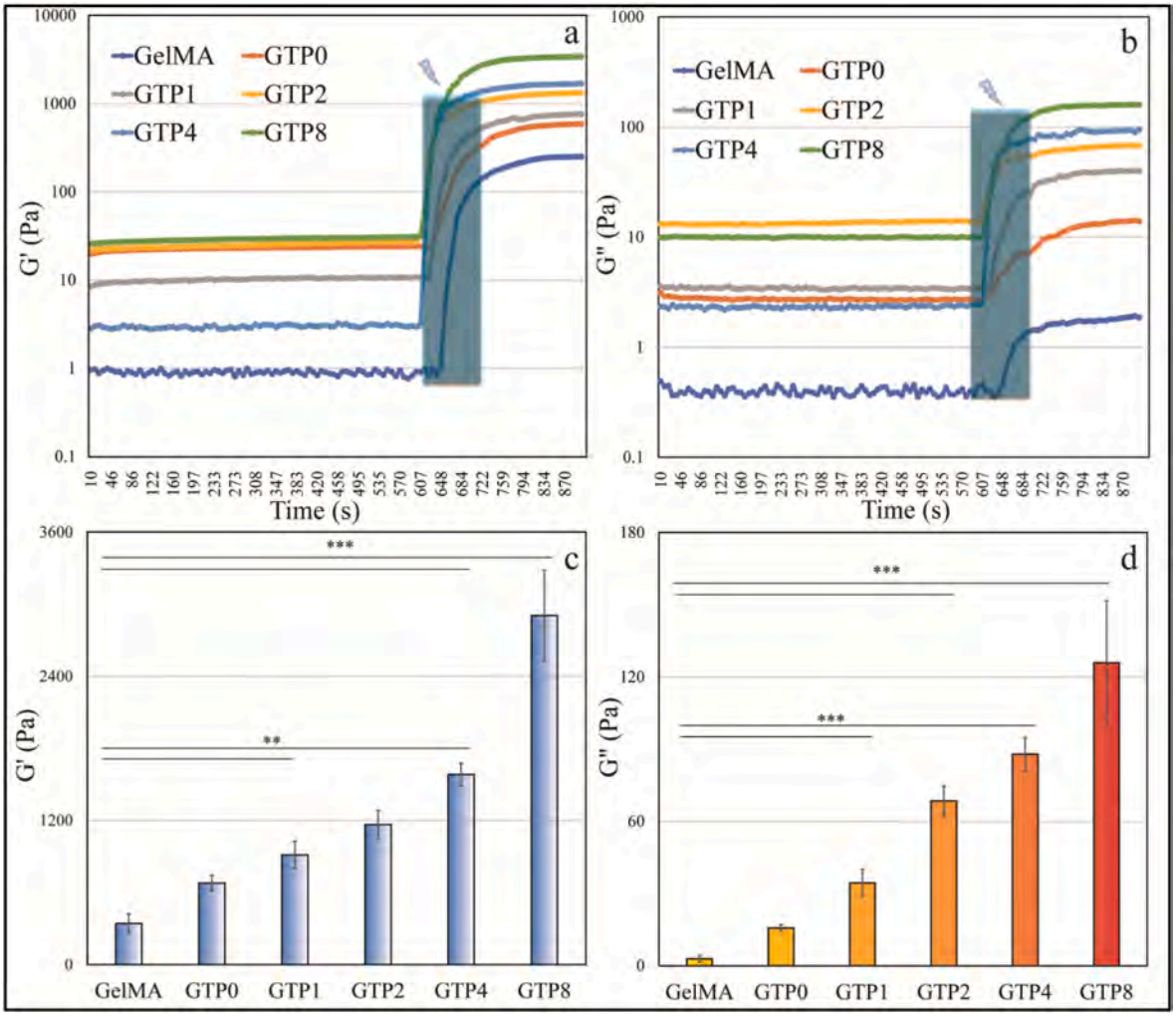

Fig. 5. Rheological test of hydrogels. **a**. The storage modulus of hydrogels. **b**. Loss modulus of hydrogels. **c.** Statistical analysis of storage modulus. **d.** Statistical analysis of loss modulus. Blue pillar means UV irradiation.

tubes with hydrogels and spread on Petri dishes containing solid culture media. Fig. 6a showed that the number of bacterial colonies in the hydrogels containing TCS was less than hydrogels without TCS. The most significant colony density occurred in the TCP, GelMA and GTP0 hydrogels. There was no significant difference between the three groups, indicating that TCP, GelMA and GTP0 groups had no apparent antibacterial property. The number of colonies of *S.aureus* and *E.coli* decreased gradually with the increase of TCS content. Once the TCS content increased to GTP4 hydrogel level, no colonies were visible in both *S.aureus* and *E. coli*. This result confirmed the antibacterial efficiency of TCS.

To further study the mechanism of TCS, bacteria morphologies were characterized. SEM results (Fig. 6b-b4 & c1-c4) showed that both bacteria, *S.aureus* (Fig. 6b1, b2) and *E.coli* (Fig. 6c1, c2), presented typical shape colonies with intact sphere and rod structure, respectively, when cultured on GelMA and GTP0 hydrogels. In comparison, bacteria colonies and structural integrity were highly affected with collapsed colonies when bacteria cultured on GTP4 (Fig. 6b3, c3) and GTP8 (Fig. 6b4, c4) hydrogels. A quantitative method was used to measure the antibacterial properties of hydrogels. The OD values of culture solutions were measured after submerging the hydrogels in *S. aureus* and *E. coli* solutions for 12 h. The results (Fig. 6d and e) showed that TCS significantly enhanced the bacterial inhibition on the hydrogels. GelMA and GTP0 hydrogels showed no antibacterial effect, while GTP1 and GTP2 showed some effect with an inhibition rate of 25.3% and 48.6% for *S. aureus* and 24.1% and 79.5% for *E. coli*, respectively. GTP4 and GTP8 hydrogels showed an improved inhibition rate of 86.4% and 99.6% for *S. aureus* and their inhibition rates for *E. coli were* 89.1% and 95% for *E. coli*, respectively. The results indicated that GTP4 and GTP8 presented better antibacterial property compared with other groups. Since infection usually happened during the wound healing process, the antibacterial property of hydrogel was necessary [2,34]. Besides, TCS was a derivative product of chitosan with better electrostatic interactions ability than chitosan, and it could react with phospholipid membrane to destroy bacteria which showed strong antibacterial effect at low concentration. There were also researches about cysteamine hydrochloride modified carboxymethyl chitosan (C-CMCS), which produced chitosan derivatives with thiol groups and possessed advantages, such as better solubilities and reaction activities. However, C-CMCS showed no evidence of antibacterial property [35,36], while carboxymethyl chitosan possessed antibacterial property against Gram negative strain as a result of its chelating capacity of di- and trivalent cations [17]. Therefore, C-CMCS may not function as an antibacterial material. In our experiment, TCS reduced the number of bacterial colonies and affected its structure integrity, showing an excellent inhibitory effect against *E.coli* and *S.aureus*, which was in consistency with previous studies [17].

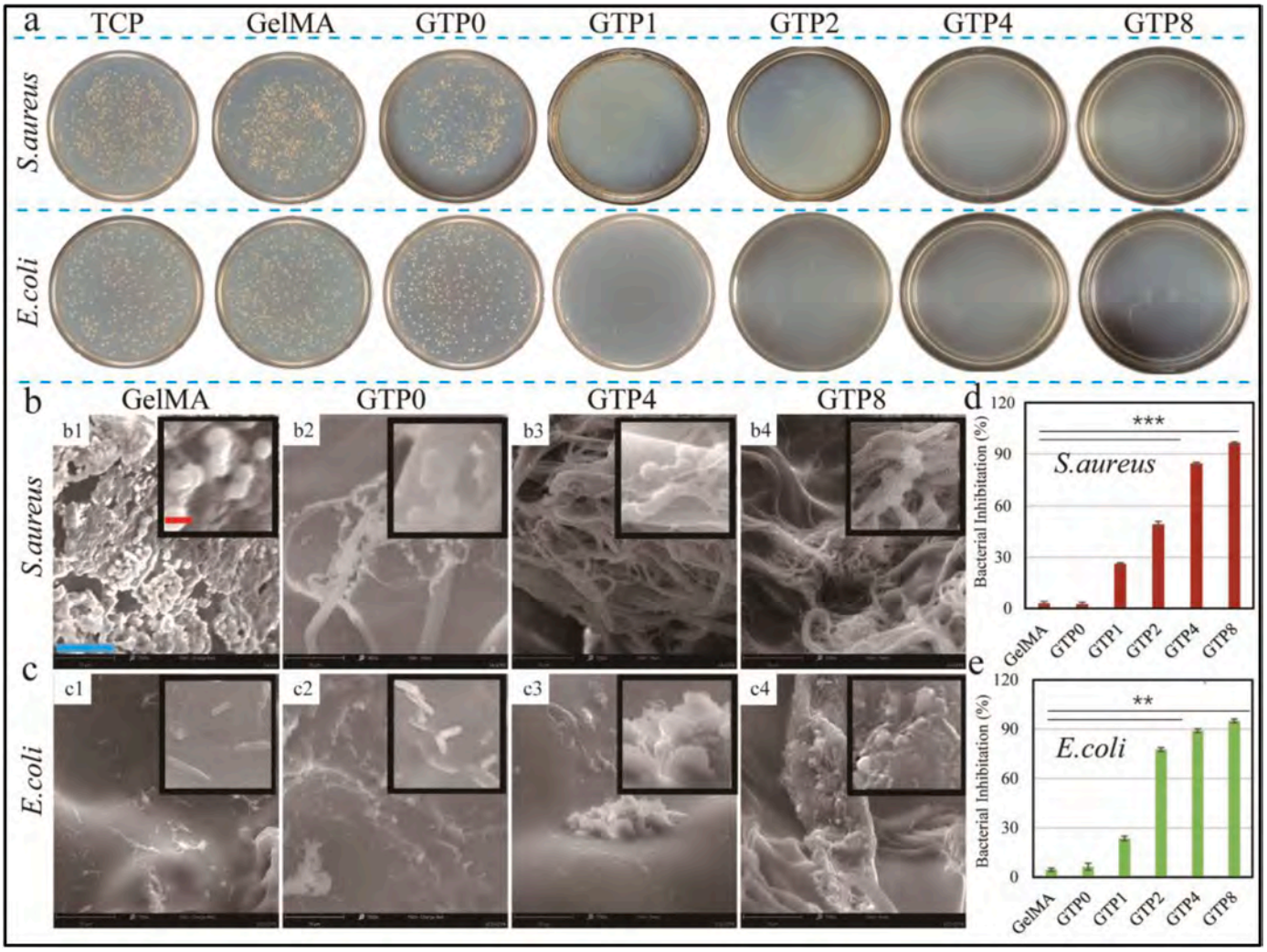

Fig. 6. Antibacterial experimental tests of hydrogels. **a.** Optical images of *S.aureus* and *E. coli*. **b1-b4.** SEM images of *S. aureus*. **c1-c4**. SEM images of *E. coli*. **d.** Bacterial inhabitation of *S.aureus*. **e.** Bacterial inhabitation of *E. coli*. Scale bar are 10 μm (blue bar) and 500 nm (red bar), respectively. (For interpretation of the references to color in this figure legend, the reader is referred to the Web version of this article.)

3.7. Antioxidant test

Free radicals generated and aggravated during wound healing process, which led to the disorder of adjacent tissues and delay of wound cicatrization [20]. Cell structures could be damaged by free radicals, including nucleic acid, protein and cell membrane. Therefore, the scavenging effect of scaffold was much needed during he wound healing. The antioxidant properties of hydrogels were determined by DPPH assay. By measuring the radical scavenging ability of hydrogels, the antioxidant property was evaluated. As shown in Fig. S3, the color of DPPH solutions faded in GTP4 and GTP8, which was the same as the positive control ascorbic acid (marked as "AA" group), while the color change in GelMA and GTP0 group were negligible. The antioxidant activity was 96.1% for AA, 20.8% for GelMA, 17.4% for GTP0, 76.3% for GTP4 and 77.9% for GTP8. Interestingly, GelMA and GTP0 groups showed certain antioxidant activity, which might result from aromatic compounds (such as tyrosine and phenylalanine) [37]. These results indicated that GTP4 & GTP8 had superior antioxidant activities, which might promote would healing.

3.8. In vitro cell culture

Cytotoxicity is one of the most critical factors for wound dressing [38]. Hydrogel cytotoxicity and cell morphology were evaluated by CCK-8 test and Live & Dead staining. Fig. 7 a-l showed that cell number in all groups increased with time. The majority was living cell (stained as green) and few dead cells were observed (stained as red). On day 1, cells represented spherical morphology (Fig. 7 a-d). On day 3 and 5, they spread well with an elongated morphology, which were more obvious in GTP0, GTP4 and GTP8 group (Fig. 7 f-h). Compared with GelMA and GTP0 groups, more cells were observed in GTP4 and GTP8 group (Fig. 7 e-h; i-l).

The CCK-8 results were in consistence with above result. Fig. 7m showed that the OD value of every group increased with time. On day 3 and day 5, GTP4 group had the highest OD value, which GelMA group had the lowest one. This result indicated that the composite hydrogel showed better proliferation than GelMA hydrogel, which was attributed to the effect of enhancing nutrients exchange by PCLPBA and proliferation by TCS. Chitosan and its derivatives were reported to enhanced cell migration and stimulates fibroblast proliferation by interacting with growth factors in the serum and potentiating their effect [39]. However, there were studies reported that high concentration of chitosan led to limited cell proliferation [40]. GTP4 showed better cell growth than GTP8, demonstrating that excessive TCS probably restrained cell growth. Fig. 7n showed that during the whole culture period, all groups had cell viabilities above 93%. This indicated that hydrogels were biocompatible, and their cytotoxicity were negligible.

3.9. In vivo experiment

Wound healing is a complex process affected by multiple factors, such as immune response, angiogenesis and collagen deposition [20]. The hydrogel was applied to the whole skin defect of adult SD rats to assess the wound healing potential of the hydrogel (Fig. 1c). Wound

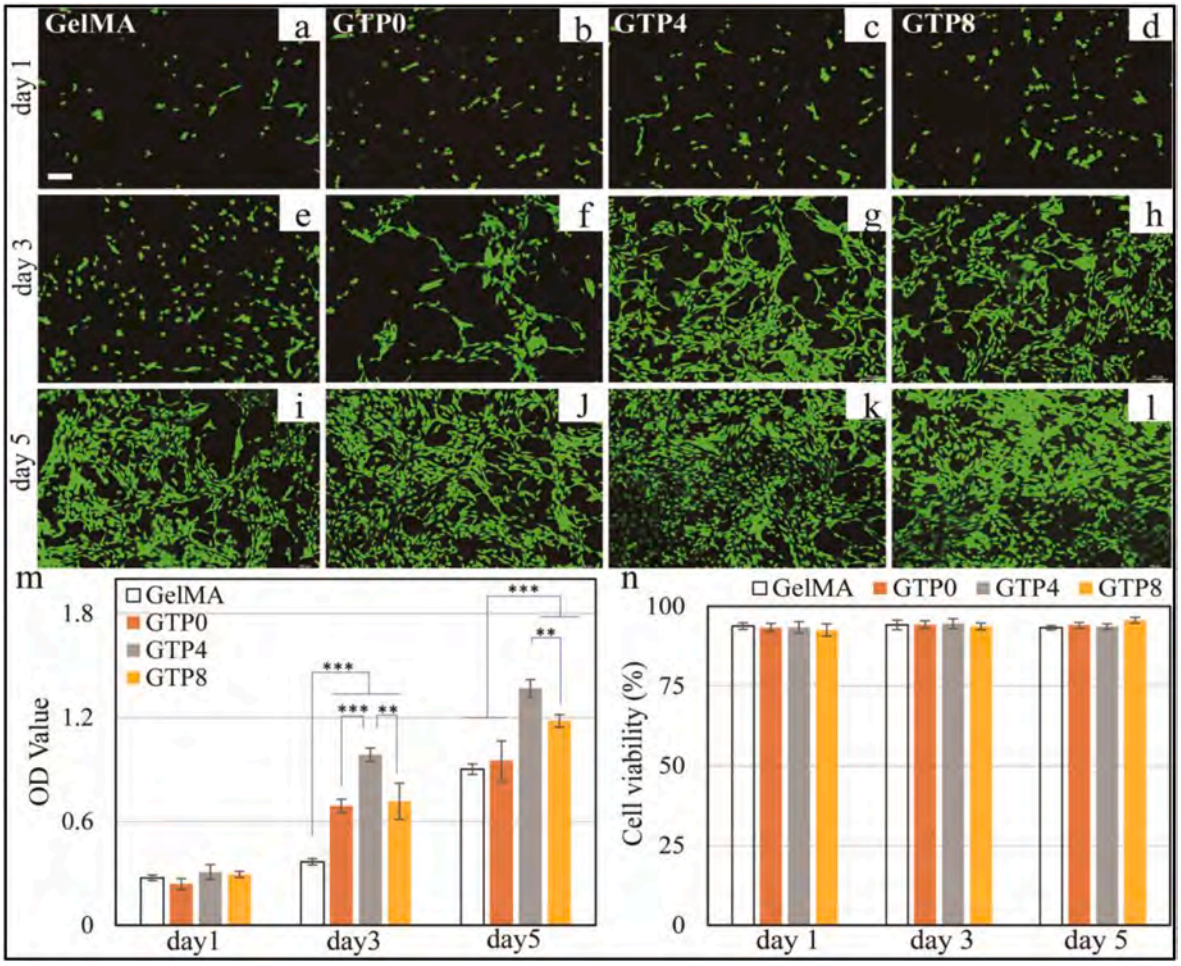

Fig. 7. NIH 3T3 cell cultured on hydrogels. **a-l**. Fluorescence images of cell on hydrogels on day 1, 3 and 5. Scale bars is 100 μm. **m**. OD values of CCK-8 test on day 1, 3 and 5, respectively. **n**. Cell viabilities at day 1, 3 and 5, respectively.

images were taken on days 7, 14 and 21 in the healing process. Results presented the wound healing process (Fig. 8a) and statistical analysis of wound area (Fig. 8b). On day 7, all wounds that were treated with hydrogels exhibited a significant difference in wound area compared with the blank group. On day 14, all wound area further decreased. On day 21, the wound area of the GTP4 group remained 2.3%, while the Blank, GelMA and GTP0 groups remained 11.0%, 10.2% and 9.2%, respectively.

Tissues samples from the wound and neighboring skin were taken to observe the regeneration activity and histological changes in untreated and treated groups. Fig. 8c is the representative image of H&E and Masson's staining taken on day 7 and day 14. Result showed that all groups depicted inflammation near the epithelium indicated with a green arrow. The redness of the skin showed the aggregation of various

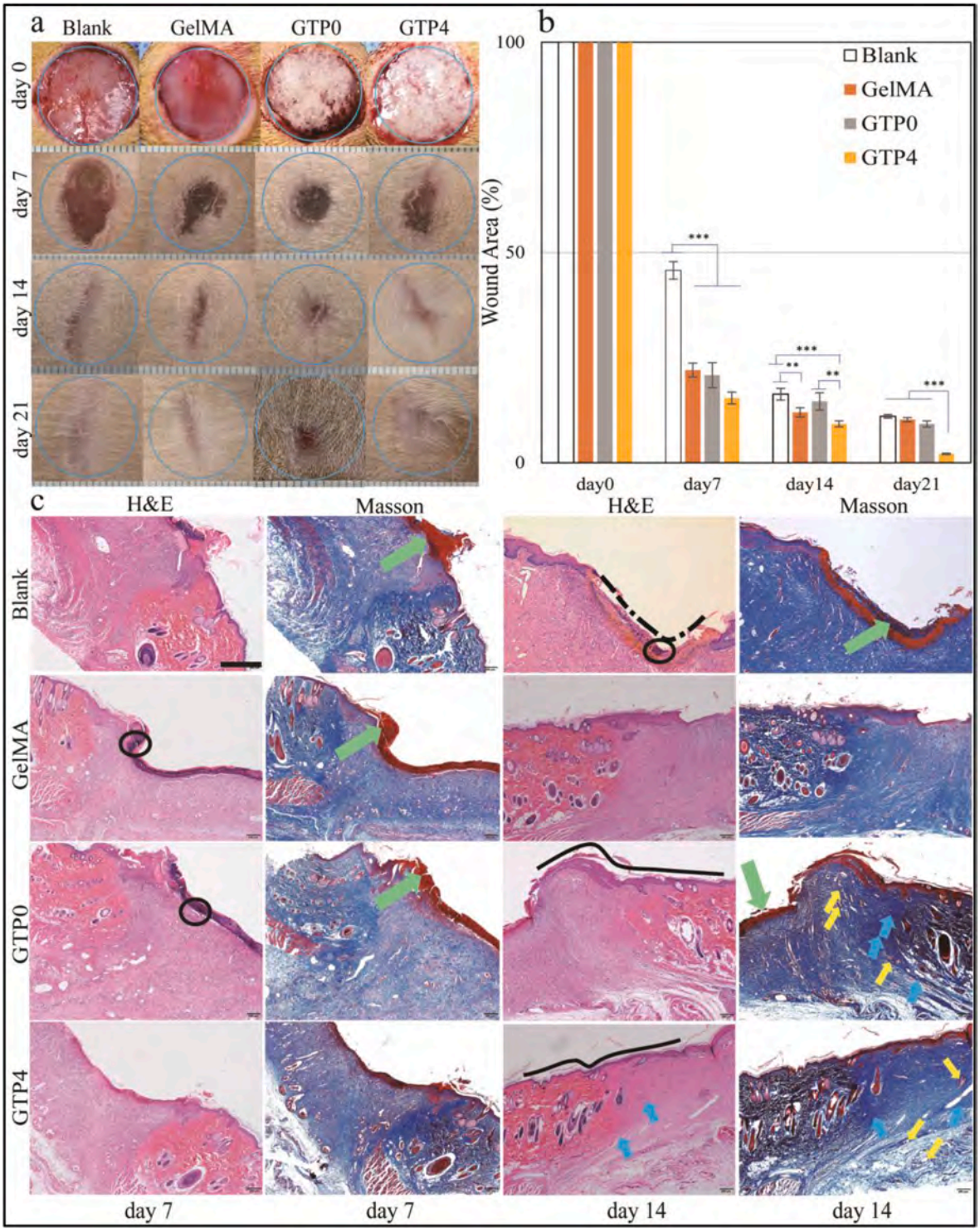

Fig. 8. Full skin defect repair in SD rats. **a**. Wound healing process. The defect size is 15 mm. **b**. Statistical analysis of wound area. **c**. Representative tissues images of H&E and Masson's staining on day 7 and day 14. Inflammation, neutrophilic infiltrated cells and the complete epithelial layer are shown at the green arrow, black circle and solid layer, respectively. An incomplete epithelial layer, collagen fibers and blood vessels are represented by the dotted layer, blue arrow and yellow arrow, respectively. The scale bar is 600 μm. (For interpretation of the references to color in this figure legend, the reader is referred to the Web version of this article.)

blood cells and clotting factors which indicated that the wound was passing through the inflammatory cycle. However, GTP4 treated wound showed reduced inflammation on day 7. The neutrophilic infiltration could be seen at the inflammation site encircled by a black circle. The redness and neutrophilic infiltration could also be observed in the untreated group on day 14, indicating that the Blank group could not overcome the inflammation. The evidence of inflammation was further strengthened by the incomplete epithelialization marked with a dotted line. Wounds treated with GTP0 and GTP4 hydrogels could form complete epithelialization, arguing the impact of treatment. Similarly, several blood vessels and collagen fibers could be seen in GTP0 and GTP4 group. The results indicated that the immune response of the GTP4 group was less on day 7, while other groups had a more apparent immune response. On day 14, both GTP0 and GTP4 groups formed complete epithelialization with newly formed vessels and collagen fiber deposition.

Fig. 9 represented the histopathological and immunochemical analysis on day 21 by H&E, Masson's and CD31 staining. Observation of the wound through H&E and Masson's staining on day 21 indicated that all the groups had formed the intact epithelial layer indicated by the red arrow. However, the quality of wound healing seemed more improved in groups treated with GTP0 and GTP4. There was a denser network of blood capillaries in these groups, especially in the GTP4 treated group indicated with yellow arrows. Moreover, collagen fiber seemed highly organized and loosely packed, showing the healing quality resulting from treatment. To draw a better comparison between newly formed tissue and neighboring healthy skin, we encircled the parts in which the yellow circle surrounded the newly formed tissue. The red circle indicated healthy skin. The comparison showed that newly regenerated skin in GTP0 and GTP4 treated group had a highly organized tissue network similar to normal skin. Moreover, a more delicate organization of collagen fiber could be observed in the GTP4 treated group. To identify the endothelial cell density in the tissue section, we used CD31 as a marker. The immunochemical staining of CD31 indicated a noticeable difference in CD31 expression in groups treated with GTP4, indicating the dense network of blood capillaries within this group.

For acute skin wounds, the components and functions of hydrogel wound dressing are vital [38,41]. GelMA is a widely used biomaterial, due to its abundance of bioactive motifs that support cell adhesion and matrix remodeling [6]. Chitosan is a natural polysaccharide, which can stimulate extracellular lysozyme activity, promote fibroblast proliferation and inhibit the formation of scar tissues [42]. TCS is a chitosan derivative with the antimicrobial ability and negligible cytotoxicity [17,43]. Besides, it can function as an antioxidant agent, reducing free radicals and promoting wound healing [23]. Hydrogel with nanofiber is reported to significantly reduce fibrosis and scar tissue formation during wound healing, while allowing cell penetration and facilitating angiogenesis [14,44]. The synergistic effect of the above materials may be the reason for the prominent wound healing effect of GTP4 hydrogel.

4. Conclusions

In this study, a novel multifunctional photo-crosslinking hydrogel@PCLPBA nanofiber was successfully prepared. The GTP4 hydrogel wound dressing has strong antibacterial property against both Gram-negative and positive bacteria, strong antioxidant property and moderate mechanical property. Besides, the GTP4 hydrogel precursor solution can be injected, photo-crosslinked *in situ* and 3D printed. Cell experiments showed that NIH 3T3 cells proliferated well on the hydrogel with orientation and high viabilities. In the SD rat models of full skin

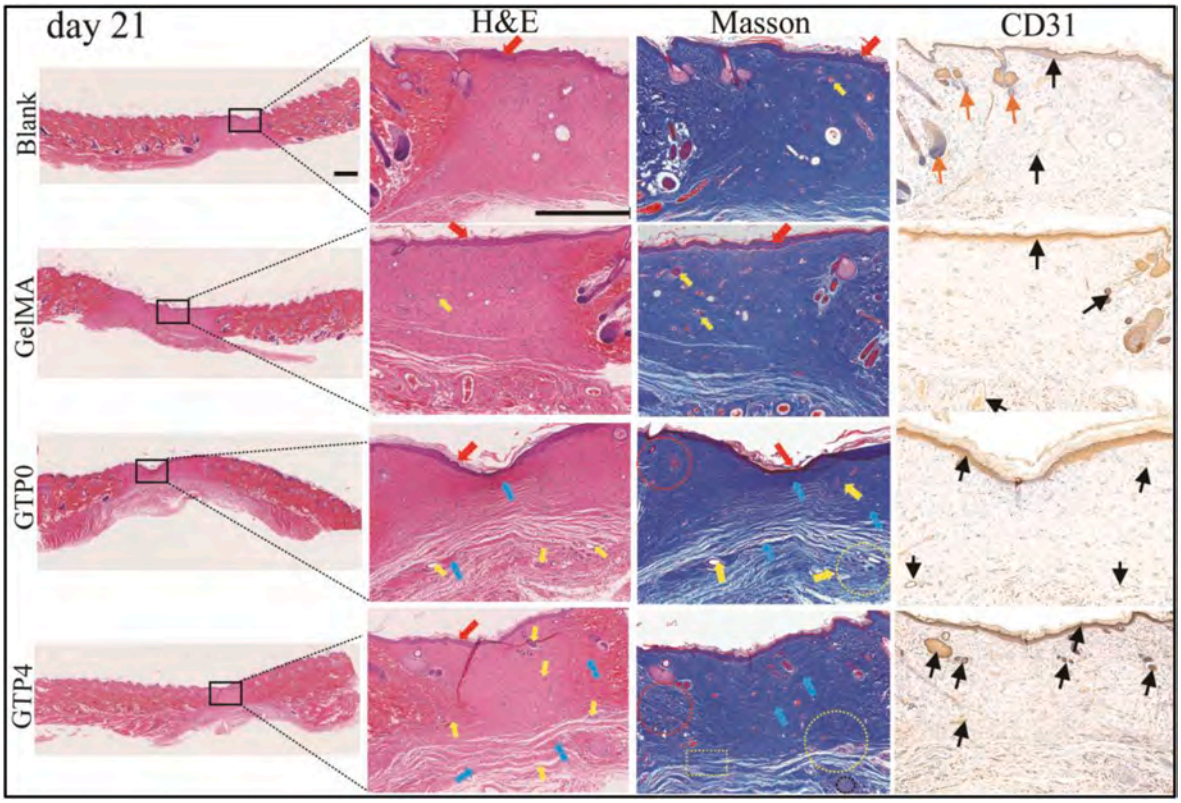

Fig. 9. Representative images of H&E, Masson's and CD31 stained tissue sections on day 21. The epithelial layer, collagen fibers and blood vessels are shown as the red arrow, blue arrow and yellow arrow, respectively. Muscles, sebaceous gland and the representative section from the newly healed area are shown as yellow dotted square, black dotted circle and yellow dotted circle, respectively. The red dotted circle represents the representative section from the neighboring skin. CD31 positive stain and CD31 counterstained are represented by a black arrow and a brown arrow, respectively. The scale bar is 800 μm. (For interpretation of the references to color in this figure legend, the reader is referred to the Web version of this article.)

defects, wound treatments with hydrogels showed a significant reduction in wound area at 7 and 14 days after surgery. The results of the histological analysis showed that the GTP4 group could promote wound healing, skin epithelialization, collagen deposition and orientation of collagen fibers on neovascularization, which has the potential as a clinical wound dressing. Future work needs to explain the mechanism of GTP4 hydrogel on wound healing, such as the production of cytokines and chemokines in wound areas.

Author statement

Fan Yu, Atta ur Rehman Khan and Yaqiang Li conceived the study and participated in the experiment design. Fan Yu performed the experiment, and Binan Zhao provided experimental technical guidance. Xianrui Xie, Mohamed EL-Newehy, Hany EL-Hamshary and Yosry Morsi analyzed experimental results. Fan Yu completed figures construction and manuscript writing. Jun Li, Jianfeng Pan and Xiumei Mo checked and revised the manuscript. All authors discussed the results and approved the final version.

Declaration of competing interest

The authors declare that they have no known competing financial interests or personal relationships that could have appeared to influence the work reported in this paper.

Data availability

The authors do not have permission to share data.

Acknowledgments

This research was supported by Science and Technology Commission of Shanghai Municipality (No. 20S31900900, 20DZ2254900), Sino German Science Foundation Research Exchange Center (M – 0263) and the Research Project of Shanghai Municipal Health Commission (No. 20194Y0316). This project was also supported by Researchers Supporting Project Number (RSP-2021/65), King Saud University, Riyadh, Saudi Arabia, National Advanced Functional Fiber Innovation Center (2021-fx020301). International Cooperation of 2021–2022 China and Poland Science and Technology Personnel Exchange Program (No.17).

Appendix A. Supplementary data

Supplementary data to this article can be found online at https://doi.org/10.1016/j.compositesb.2022.110294.

References

[1] Meng Z, Zhou D, Gao Y, et al. miRNA delivery for skin wound healing. Adv Drug Deliv Rev 2018;129:308–18.
[2] Zhang H, Guo M, Zhu T, et al. A careob-like nanofibers with a sustained drug release profile for promoting skin wound repair and inhibiting hypertrophic scar. Compos B Eng 2022;236:109790.
[3] Li S, Deng R, Zou X, et al. Development and fabrication of co-axially electrospun biomimetic periosteum with a decellularized periosteal ECM shell/PCL core structure to promote the repair of critical-sized bone defects. Compos B Eng 2022; 234:109620.
[4] Kus KJ, Ruiz ES. Wound dressings–a practical review. Curr Dermatol Rep 2020: 1–11.
[5] Koh RH, Jin Y, Kang B-J, et al. Chondrogenically primed tonsil-derived mesenchymal stem cells encapsulated in riboflavin-induced photocrosslinking collagen-hyaluronic acid hydrogel for meniscus tissue repairs. Acta Biomater 2017; 53:318–28.
[6] Yang Z, Ren X, Liu Y. N-halamine modified ceria nanoparticles: antibacterial response and accelerated wound healing application via a 3D printed scaffold. Compos B Eng 2021;227:109390.
[7] You S, Li J, Zhu W, et al. Nanoscale 3D printing of hydrogels for cellular tissue engineering. J Mater Chem B 2018;6:2187–97.
[8] Lu M, Liu Y, Huang Y-C, et al. Fabrication of photo-crosslinkable glycol chitosan hydrogel as a tissue adhesive. Carbohydr Polym 2018;181:668–74.
[9] Berkovitch Y, Seliktar D. Semi-synthetic hydrogel composition and stiffness regulate neuronal morphogenesis. Int J Pharm (Amst) 2017;523:545–55.
[10] Liu C, Chiang B, Mejia DL, et al. Mammary fibroblasts remodel fibrillar collagen microstructure in a biomimetic nanocomposite hydrogel. Acta Biomater 2019;83: 221–32.
[11] Ngo MT, Harley BA. The influence of hyaluronic acid and glioblastoma cell coculture on the formation of endothelial cell networks in gelatin hydrogels. Adv Health Mater 2017;6:1700687.
[12] Teodorescu M, Bercea M, Morariu S. Biomaterials of poly (vinyl alcohol) and natural polymers. Polym Rev 2018;58:247–87.
[13] Liu H, Wang H, Lu X, et al. Electrospun structural nanohybrids combining three composites for fast helicide delivery. Adv Compos Hybrid Mater 2022:1–13.
[14] Li X, Cho B, Martin R, et al. Nanofiber-hydrogel composite–mediated angiogenesis for soft tissue reconstruction. Sci Transl Med 2019;11.
[15] Jin Q, Fu Y, Zhang G, et al. Nanofiber electrospinning combined with rotary bioprinting for fabricating small-diameter vessels with endothelium and smooth muscle. Compos B Eng 2022;234:109691.
[16] Meng L, Turner APF, Mak WC. Modulating electrode kinetics for discrimination of dopamine by a PEDOT:COOH interface doped with negatively charged tricarboxylate. ACS Appl Mater Interfaces 2019;11:34497–506.
[17] Geisberger G, Gyenge EB, Hinger D, et al. Chitosan-thioglycolic acid as a versatile antimicrobial agent. Biomacromolecules 2013;14:1010–7.
[18] Hou X, Chen Y, Chen F, et al. The hydroxyapatite microtubes enhanced GelMA hydrogel scaffold with inner "pipeline framework" structure for bone tissue regeneration. Compos B Eng 2022;228:109396.
[19] Xu X, Wang X, Qin C, et al. Silk fibroin/poly-(L-lactide-co-caprolactone) nanofiber scaffolds loaded with Huangbai Liniment to accelerate diabetic wound healing. Colloids Surf, B 2021;199. 111557–111557.
[20] Li J, Fang W, Hao T, et al. An anti-oxidative and conductive composite scaffold for cardiac tissue engineering. Compos B Eng 2020;199:108285.
[21] Noshadi I, Hong S, Sullivan KE, et al. In vitro and in vivo analysis of visible light crosslinkable gelatin methacryloyl (GelMA) hydrogels. Biomater Sci 2017;5: 2093–105.
[22] Xu W, Wang Z, Liu Y, et al. Carboxymethyl chitosan/gelatin/hyaluronic acid blended-membranes as epithelia transplanting scaffold for corneal wound healing. Carbohydr Polym 2018;192:240–50.
[23] Gout I. Coenzyme A: a protective thiol in bacterial antioxidant defence. Biochem Soc Trans 2019;47:469–76.
[24] Zhang F, King MW. Biodegradable polymers as the pivotal player in the design of tissue engineering scaffolds. Adv Healthc Mater 2020;9:1901358.
[25] Wang X, Jiang M, Zhou Z, et al. 3D printing of polymer matrix composites: a review and prospective. Compos B Eng 2017;110:442–58.
[26] Podstawczyk D, Skrzypczak D, Połomska X, et al. Preparation of antimicrobial 3D printing filament: in situ thermal formation of silver nanoparticles during the material extrusion. Polym Compos 2020;41:4692–705.
[27] Zhang W, Shi W, Wu S, et al. 3D printed composite scaffolds with dual small molecule delivery for mandibular bone regeneration. Biofabrication 2020;12: 35020.
[28] Chai N, Zhang J, Zhang Q, et al. Construction of 3D printed constructs based on microfluidic microgel for bone regeneration. Compos B Eng 2021;223:109100.
[29] Ma R, Wang Y, Qi H, et al. Nanocomposite sponges of sodium alginate/graphene oxide/polyvinyl alcohol as potential wound dressing: in vitro and in vivo evaluation. Compos B Eng 2019;167:396–405.
[30] Liu D, Qiu J, Xu R, et al. β-CD/PEI/PVA composite hydrogels with superior self-healing ability and antibacterial activity for wound healing. Compos B Eng 2022; 238:109921.
[31] Tytgat L, Markovic M, Qazi TH, et al. Photo-crosslinkable recombinant collagen mimics for tissue engineering applications. J Mater Chem B 2019;7:3100–8.
[32] Modaresifar K, Hadjizadeh A, Niknejad H. Design and fabrication of GelMA/chitosan nanoparticles composite hydrogel for angiogenic growth factor delivery. Artif Cell Nanomed Biotechnol 2017;46(8):1–10.
[33] Klotz BJ, Gawlitta D, Rosenberg A, et al. Gelatin-methacryloyl hydrogels: towards biofabrication-based tissue repair. Trends Biotechnol 2016;34:394–407.
[34] Qiu W, Wang Q, Li M, et al. Peptidoglycan-inspired peptide-modified injectable hydrogels with enhanced elimination capability of bacterial biofilm for chronic wound healing. Compos B Eng 2021;227:109402.
[35] Wang S, Ji X, Chen S, et al. Study of double-bonded carboxymethyl chitosan/cysteamine-modified chondroitin sulfate composite dressing for hemostatic application. Eur Polym J 2022;162:110875.
[36] Song P, Song N, Li L, et al. Angiopep-2-modified carboxymethyl chitosan-based pH/reduction dual-stimuli-responsive nanogels for enhanced targeting glioblastoma. Biomacromolecules 2021;22(7):2921–34.
[37] Yoon S, Ji SC, Yang J, et al. Ursodeoxycholic acid improves liver function via phenylalanine/tyrosine pathway and microbiome remodelling in patients with liver dysfunction. Sci Rep-UK 2018;8:1–11.
[38] Wang Q, Zhou S, Wang L, et al. Bioactive silk fibroin scaffold with nanoarchitecture for wound healing. Compos B Eng 2021;224:109165.
[39] Zhang Q, Qiao Y, Zhu J, et al. Electroactive and antibacterial surgical sutures based on chitosan-gelatin/tannic acid/polypyrrole composite coating. Compos B Eng 2021;223:109140.
[40] Wahid F, Zhou Y-N, Wang H-S, et al. Injectable self-healing carboxymethyl chitosan-zinc supramolecular hydrogels and their antibacterial activity. Int J Biol Macromol 2018;114:1233–9.
[41] Wang Y, Xiao D, Yu H, et al. Asymmetric composite wound dressing with hydrophobic flexible bandage and tissue-adhesive hydrogel for joints skin wound healing. Compos B Eng 2022;235:109762.

[42] Cao S, Xu G, Li Q, et al. Double crosslinking chitosan sponge with antibacterial and hemostatic properties for accelerating wound repair. Compos B Eng 2022;234:109746.
[43] Li J, Li L, Lv J, et al. Preparation of thiolated chitosan/silver nanowire composite hydrogels with antimicrobial activity for obstetric wound care. Mater Lett 2020;280:128497.
[44] Qiu W, Wang Q, Li M, et al. 3D hybrid scaffold with aligned nanofiber yarns embedded in injectable hydrogels for monitoring and repairing chronic wounds. Compos B Eng 2022;234:109688.